Journal of Biomechanics 45 (2012) 2673–2679

Contents lists available at SciVerse ScienceDirect

Journal of Biomechanics

journal homepage: www.elsevier.com/locate/jbiomech
www.JBiomech.com

Compressive properties of passive skeletal muscle—The impact of precise sample geometry on parameter identification in inverse finite element analysis

Markus Böl [a,*], Roland Kruse [a], Alexander E. Ehret [a], Kay Leichsenring [b], Tobias Siebert [b]

[a] Institute of Solid Mechanics, Technische Universität Braunschweig, 38106 Braunschweig, Germany
[b] Institute of Motion Science, Friedrich Schiller University Jena, 07749 Jena, Germany

ARTICLE INFO

Article history:
Accepted 15 August 2012

Keywords:
Rabbit soleus muscle
Parameter identification
Optical measurements
Passive muscle properties
Static friction coefficient

ABSTRACT

Due to the increasing developments in modelling of biological material, adequate parameter identification techniques are urgently needed. The majority of recent contributions on passive muscle tissue identify material parameters solely by comparing characteristic, compressive stress–stretch curves from experiments and simulation. In doing so, different assumptions concerning e.g. the sample geometry or the degree of friction between the sample and the platens are required. In most cases these assumptions are grossly simplified leading to incorrect material parameters. In order to overcome such oversimplifications, in this paper a more reliable parameter identification technique is presented: we use the inverse finite element method (iFEM) to identify the optimal parameter set by comparison of the compressive stress–stretch response including the realistic geometries of the samples and the presence of friction at the compressed sample faces. Moreover, we judge the quality of the parameter identification by comparing the simulated and experimental deformed shapes of the samples. Besides this, the study includes a comprehensive set of compressive stress–stretch data on rabbit soleus muscle and the determination of static friction coefficients between muscle and PTFE.

1. Introduction

From the mechanical perspective, biological tissues are challenging materials that can be roughly characterised to be constant in volume, highly non-linear, viscoelastic, and anisotropic. Thus, it is not surprising that experiments on these tissues are challenging, too. A particular aspect in this context is the determination of the specimen shape during sampling. As biological tissues are very soft they are often mechanically tested in compression setups. Hereby, the specimen is located between two platens, where one of them is force/displacement controlled moving against the other one. In the unlikely case that there is no friction between the platens and the sample, the test can be referred to as unconstrained and the deformation results in a uniaxial compression state. Provided that the specimen consists of a homogeneous material, the test leads to a homogeneous state of deformation, i.e. the deformation gradient $\boldsymbol{F}=\partial\boldsymbol{x}/\partial\boldsymbol{X}$ is independent of the position $\boldsymbol{X}$ (e.g. Ogden, 1997). However, as it is almost impossible to prepare frictionless surfaces the compression test will generally lead to inhomogeneous deformation states, e.g. manifested by barrelling of the specimen (Miller, 2001, 2005; Morriss et al., 2008). In such a situation, the deformation must be considered to be constrained. For small deformations of an isotropic material, Miller (2005) developed a method to describe such situations analytically. However, as we focus on anisotropic muscle tissues undergoing large deformations, this approach is insufficient.

Isolated muscle tissue samples have been studied experimentally in compression (McElhaney, 1966; Aimedieu et al., 2003; Van Loocke et al., 2006, 2008, 2009; van Sligtenhorst and Cronin, 2006; Song et al., 2007; Chawla et al., 2009), shear (van Turnhout et al., 2005), and tension experiments (Yoo et al., 2009; Calvo et al., 2010; Nie et al., 2011). If such experiments are interpreted by constitutive models, the parameter identification is usually based on a simplified analytical solution of the problem and only the stress response is taken into account.

As an improved strategy, we suggest in this contribution to use the iFEM for parameter estimation, including the exact sample geometries and the presence of friction at the compressed specimen faces. Moreover, the simulated and experimental deformed shapes of the samples are used as additional information to assess the quality of the parameter identification procedure.

2. Materials and methods

2.1. Sample preparation and testing

All experiments were approved according to section 8 of the German Animal Protection Law (Tierschutzgesetz BGBl. I 1972, 1277).

* Corresponding author. Tel.: +49 531 391 7052; fax: +49 531 391 7053.
E-mail address: m.boel@tu-bs.de (M. Böl).

0021-9290/$ - see front matter © 2012 Elsevier Ltd. All rights reserved.
http://dx.doi.org/10.1016/j.jbiomech.2012.08.023

Table 1
Summarised geometrical sample information. V (mm^3) denotes the volume of the specimen, h (mm) is the undeformed height of the sample, $A_\phi = V/h$ (mm^2) is the average cross-sectional area perpendicular to the loading direction, and $\boldsymbol{m}$ describes the mean fibre direction vector, optically measured in the specimen , whereby the components in x-, y-, and z-direction are given. In addition $\alpha_{\boldsymbol{m}}$ is the orientation angle between the loading direction and the y-axis, see also Fig. 7. Mark '–': due to the dimension of the muscle no measurement was performed for this loading direction.

Tissue set no.	0°					45°					90°				
	V	h	A_ϕ	$\boldsymbol{m}$	$\alpha_{\boldsymbol{m}}$	V	h	A_ϕ	$\boldsymbol{m}$	$\alpha_{\boldsymbol{m}}$	V	h	A_ϕ	$\boldsymbol{m}$	$\alpha_{\boldsymbol{m}}$
I	53.8	3.1	17.7	0.02/−0.97/0.23	14	116.9	4.2	28.2	−0.14/0.55/0.83	57	110.6	3.3	33.7	0.3/−0.07/−0.95	86
II	–	–	–	–	–	167.6	4.9	34.3	−0.44/−0.52/−0.72	59	62.0	2.7	23.0	−0.92/−0.02/0.39	89
III	63.8	3.6	17.6	−0.12/0.98/−0.08	11	141.6	4.9	29.1	−0.74/−0.56/−0.34	−56	57.3	2.7	21.4	0.87/0.08/0.45	85
IV	–	–	–	–	–	122.0	3.9	31.6	0.61/−0.59/0.53	54	91.4	3.2	28.3	0.53/0.16/0.83	81
V	–	–	–	–	–	109.7	4.1	27.0	−0.15/0.42/−0.89	66	108.3	4.8	22.7	−0.98/0.13/−0.08	83
VI	–	–	–	–	–	116.9	4.9	24.0	−0.09/0.79/0.59	38	165.0	4.4	37.2	−0.76/0.06/0.64	87
VII	64.7	4.1	15.8	−0.34/0.9/−0.07	26	128.4	5.2	24.9	0.89/−0.41/0.15	66	52.5	3.6	14.5	0.3/0.04/−0.95	88
VIII	93.9	3.4	27.7	0.28/0.96/0.03	16	127.4	3.8	34.0	0.59/0.8/0.11	37	144.7	4.0	36.6	−1.0/0.0/0.2	87
IX	77.2	3.8	20.2	−0.14/0.96/−0.07	11	147.7	4.7	31.3	0.71/−0.56/−0.43	56	163.5	4.3	38.5	−0.03/0.03/1.0	88
X	77.5	3.0	25.6	0.07/0.96/−0.26	16	122.3	5.3	23.1	−0.37/0.58/0.72	55	79.2	3.4	23.6	0.99/0.09/−0.14	85
XI	101.8	4.1	25.1	0.03/1.0/0.01	0	114.3	4.0	28.9	−0.68/0.52/0.51	59	–	–	–	–	–
XII	57.5	3.1	18.8	0.51/0.84/−0.16	33	80.3	3.7	21.6	0.81/0.58/−0.04	54	95.0	4.0	23.7	−0.04/−0.04/1.0	88
XIII	71.0	2.9	24.6	−0.09/0.95/0.29	18	–	–	–	–	–	85.8	3.4	25.7	0.1/−0.07/1.0	86
XVI	–	–	–	–	–	62.1	2.8	22.0	0.03/−0.8/−0.61	38	54.8	3.4	16.0	0.45/0.09/−0.88	85
XV	–	–	–	–	–	130.8	3.2	40.5	−0.05/0.59/−0.81	54	161.8	4.6	35.0	0.98/0.19/0.09	79
Mean ± s.d.					**14 ± 6.9°**					**53.5 ± 9.1°**					**85.6 ± 2.7°**

Thirty-seven cubic muscle samples with characteristic edge lengths between 3 and 6 mm were cut from soleus muscles ($n=15$, Table 1) of New Zealand white rabbits using a holder assembled with a razor blade, c.f. Remark 1. These samples were subjected to constrained compression tests, performed on a universal testing machine (Zwick Z010, Zwick GmbH & Co. Ulm, Germany), up to 45% at a quasi-static strain rate of 0.05% s^{-1} in line with the protocol by Van Loocke et al. (2006). While the displacement u of the upper platen was predefined, the resulting force F was measured and converted to mean engineering stress $P=F/A_\phi$ by division through the average cross-sectional area A_ϕ. The axial compressive stretch $\lambda=1+u/h$ was calculated from u and the undeformed sample height h. Specimens with three different, optically estimated mean fibre orientations (0°, 45°, and 90°) with respect to the loading direction were considered. Information on sample geometries and loading directions are summarised in Table 1. In order to diminish friction effects, polytetrafluoroethylene (PTFE) platens combined with different lubricants were used. As a result of secondary tests, silicone oil was used for the final experiments (Fig. 5) since a small static friction coefficient of $f_{SO}=0.02$ could be obtained (Remark 2).

In order to measure the three-dimensional tissue shape during deformation, the optical measurement system ARAMIS (GOM mbH Braunschweig, Germany) was used. Accordingly, the surfaces of the samples were coated with single points of black and white varnish (Fig. 1). As this random pattern deforms simultaneously with the tissue, the deformation can be recorded by a sensor including two CCD cameras, each of them providing 8-bit images with a resolution of 2352 (horizontal) × 1728 (vertical) pixels (pixel size: 10 μm × 10 μm) in TIFF format. A special revolvable holder as shown in Fig. 1 was used to rotate the sample by 360° in steps of 72°. Five single images of the tissue surface were recorded within a time span of 5 s. The random pattern on the sample surface and a calibrated marker pattern on the PTFE block below the sample allow to align and combine the images into a three-dimensional shape. A representative example of these outcomes is given in Fig. 2. In (a) the reconstructed undeformed shape and in (b) the surface of the same sample at maximum deformation are displayed.

Remark 1 (*Initial muscle tissue geometry*)**.** The small dimensions of the rabbit soleus limited the specimen size to approximately 3–6 mm edge length. However, due to the high mobility of fresh muscle tissue and the small dimensions it was nearly impossible to cut perfectly cuboid geometries without manipulation that may create undesired fixation and preparation effects (c.f. Hollenstein et al., 2011). To avoid this, we accepted cuboid-like samples. A typical example is illustrated in Fig. 2(a).

Remark 2 (*Determination of the static friction coefficient*)**.** The static friction coefficient $f=F_F/F_N$ is the ratio between normal F_N and friction force F_F between two non-moving bodies (Fig. 3(a)). It can be estimated by controlling F_N and measuring the maximum F_F before the body starts moving using a spring scale (e.g. Shacham et al., 2010). We cut 26 strips from soleus muscles of New Zealand white rabbits, placed them on a PTFE sheet and increased F_N stepwise while measuring F_F. Two different lubricants were used: physiological saline solution (PSS) and silicone oil (SO). The results are illustrated in Fig. 3. For SO a small mean static friction coefficient of $f_{SO}=0.02\pm0.006$ was determined, c.f. Fig. 3(b), whereas for PSS $f_{PSS}=0.48\pm0.03$ indicates much worse sliding characteristics, see Fig. 3(a). Due to the negligible influence of F_N (Fig. 3), we assume f to be constant.

2.2. Mathematical modelling

The microstructure of skeletal muscle tissue is characterised by densely packed muscle fibres, which are arranged in fascicles. A high content of water leads to nearly incompressible material behaviour (Baskin and Paolini, 1967). Since the fibres locally follow a predominant unidirectional alignment, transverse isotropy with respect to the direction of this alignment can be assumed. Thus, a transversely isotropic, hyperelastic material model (Holzapfel et al., 2000) with the extension to slightly dispersed fibres by Gasser et al. (2006) was used to describe the passive behaviour of muscle tissue. Accordingly, the strain-energy function

$$\psi=\psi_g+\psi_f \tag{1}$$

is additively decomposed in an isotropic (ψ_g) and a transversely isotropic contribution (ψ_f). The non-collagenous ground matrix is modelled as isotropic neo-Hookean material

$$\psi_g=\frac{\mu}{2}(I_1-3). \tag{2}$$

Herein, the shear modulus is denoted by μ and $I_1=\mathrm{tr}\,\boldsymbol{C}$ is the first invariant of the right Cauchy–Green tensor $\boldsymbol{C}$. The second part (Gasser et al., 2006)

$$\Psi_{c,i}=\begin{cases}\frac{c_1}{2c_2}[\exp\{c_2[\kappa I_1+(1-3\kappa)I_4-1]^2\}-1] & \text{if } I_4\geq 1\\ 0 & \text{else,}\end{cases} \tag{3}$$

characterises the collagen behaviour. The fourth invariant $I_4=\boldsymbol{m}\,\boldsymbol{C}\,\boldsymbol{m}$ depends on the preferred muscle fibre direction $\boldsymbol{m}$. Further, c_1 is a stress-like and c_2 a dimensionless parameter to be identified from experiments. The dispersion parameter $0\leq\kappa\leq 1/3$

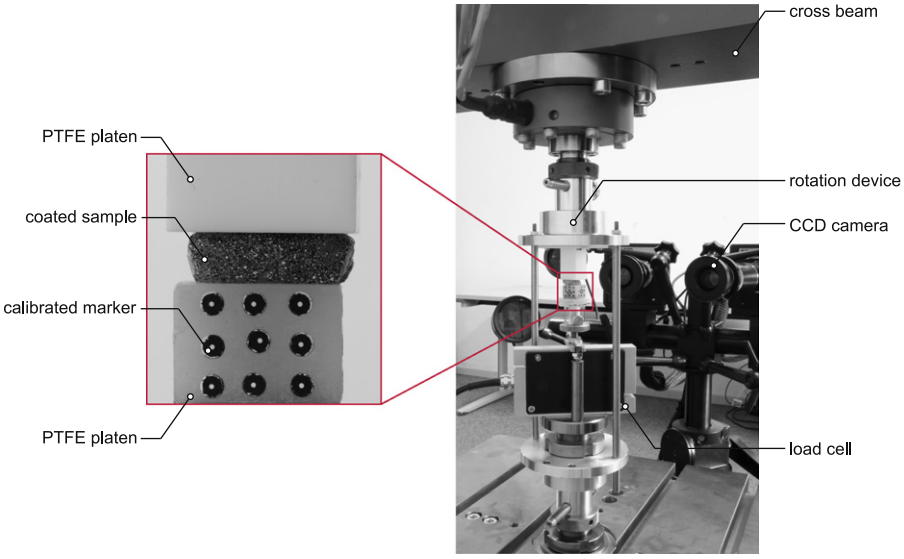

Fig. 1. Custom made rotating holder. The subfigure illustrates a close-up picture of a compressed muscle sample.

scales between perfectly aligned $\kappa = 0$ and randomly distributed fibres $\kappa = 1/3$ (Gasser et al., 2006) and can be connected to histological tissue analyses. Within this study, however, κ was used as an additional fitting parameter.

2.3. Inverse FEM

The inverse finite element method (iFEM) has been applied successfully for parameter identification of soft tissues (e.g. Samur et al., 2007; Nava et al., 2008; Ahn and Kim, 2010). Its basic idea is the coupling of a forward FE-analysis with an optimisation algorithm that finds the optimal parameter set by minimising the error between the experimental measurement and simulated response. In Fig. 4 the cardinal algorithm is illustrated. Starting with the initial geometry and an initial parameter set Fig. 4$_{(i)}$ a first FE-analysis is realised leading to a deformed geometry and a force-displacement relation, c.f. Fig. 4$_{(ii)}$. The agreement between simulated Fig. 4$_{(ii)}$ and experimental Fig. 4$_{(iii)}$ data is evaluated by the objective function

$$\mathcal{O}(\boldsymbol{p}) = \sum_{j=1}^{m}\sum_{i=1}^{n} \frac{\sqrt{({}^{j}F_i^{exp} - {}^{j}F_i^{sim})^2}/{}^{j}F_i^{exp}}{mn}, \tag{4}$$

which represents the relative square error per data point, see also Fig. 4$_{(iv)}$. Herein, ${}^{j}F_i^{exp}$ and ${}^{j}F_i^{sim}$ are the orientation dependent measured and simulated force values for every deformation increment, respectively. Further, $n = 100$ is the number of data points and $m = 3$ accounts for the three different fibre orientations, i.e. $0^\circ/45^\circ/90^\circ$. To find an optimal parameter set (vii) in terms of the parameter vector $\boldsymbol{p} = (\mu, c_1, c_2, \kappa)^T$ the objective function was minimised by means of the Nelder–Mead simplex method (Nelder and Mead, 1965; Lagarias et al., 1998). Using this algorithm, parameter sets were considered optimal when the objective function changed by less than the tolerance of 10^{-4} between two consecutive fitting steps. Furthermore, the surfaces at 0% and at 45% compressive strain obtained in the simulations were compared with the geometric data from the optical measurements.

2.4. Idealised simulations

In a next step the original geometry of the samples was approximated by cuboids with same volume V and average cross-sectional area A_ϕ, see Table 1. Using the material model with the parameters obtained from the above described optimisation procedure (Table 2), the compression experiments were simulated with the idealised cubic sample geometry. To highlight the influence of friction, we accomplished simulations for $f = 0.0$, the experimental conditions $f_{SO} = 0.02$, and also for an obviously wrong static friction coefficient, namely $f_{PSS} = 0.48$.

3. Results

3.1. Compressive stress–stretch behaviour

Rooted on fifteen tissue sets, see Table 1, 37 characteristic compressive stress–stretch responses, in dependence on the tissues' fibre alignment are presented in Fig. 5. The stiffest tissue response is obtained when the muscle fibres are oriented perpendicular to the loading direction, i.e. 90° (Fig. 5(c)) followed by a fibre orientation of 45°. Parallel alignment of loading and fibre direction, i.e. 0°, yielded the softest response. As usual for testing of soft biological tissues the specimens displayed scatter in the data. However, in view of the high level of compression applied in this study the average relative standard deviations are small and take values of 0.63, 0.68, and 0.44 for the fibre directions 0°, 45°, and 90°, respectively.

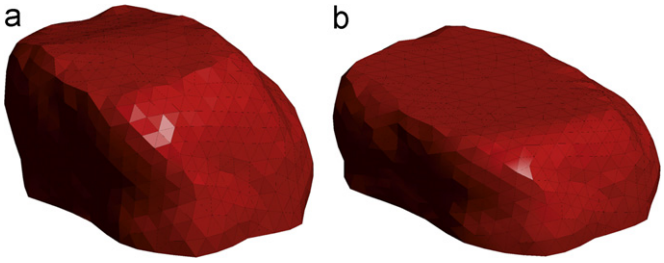

Fig. 2. Reconstructed geometries, (a) before deformation and (b) at maximum deformation of 45% compression.

3.2. FEM simulations

Applying the parameter identification technique as described in Section 2.3, 15 optimised parameter sets were determined (Table 2). The maximum relative square error turns out to be 4% which is an acceptable value when working with biological tissues. In order to exemplify the identification technique, sample I was selected randomly from the tissue set. Thus, in Fig. 6 the experimental compressive stress–stretch behaviour is compared to the stress responses Fig. 6$_{(i)}$ from the iFEM analyses using the optimised parameters of tissue set I (Table 2). In addition, Fig. 6 also displays the results obtained when compressing the idealised cuboid specimen without friction (Fig. 6$_{(ii)}$), with $f_{SO} = 0.02$ (Fig. 6$_{(iii)}$) and $f_{PSS} = 0.48$ (Fig. 6$_{(iv)}$). Expectedly, for all three fibre orientations the force responses clearly deviate from the experimental results, which confirms the limited applicability of such oversimplifications. Even if the same static friction coefficient $f_{SO} = 0.02$ is applied as for the experiments, see Fig. 6$_{(iii)}$, the compressive stress–stretch curves cannot be reproduced in a satisfying manner; particularly for the 90° fibre orientation the deviation to the experiments becomes even larger.

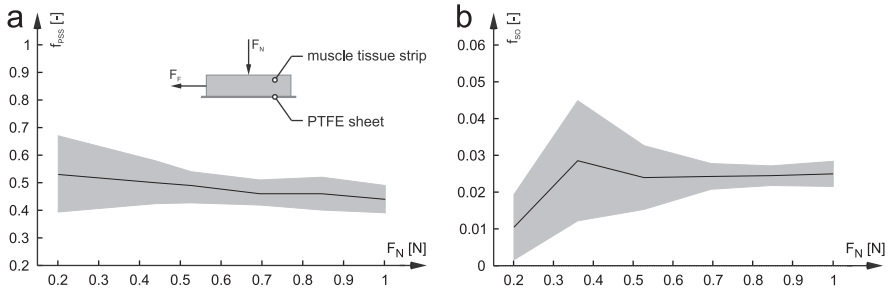

Fig. 3. Illustration of the determined static friction coefficient using (a) physiological saline solution and (b) silicone oil as lubricant versus the predefined normal load F_N including the tissues' dead weight. The black curves indicate the mean value whereas the light grey area depicts the standard deviation.

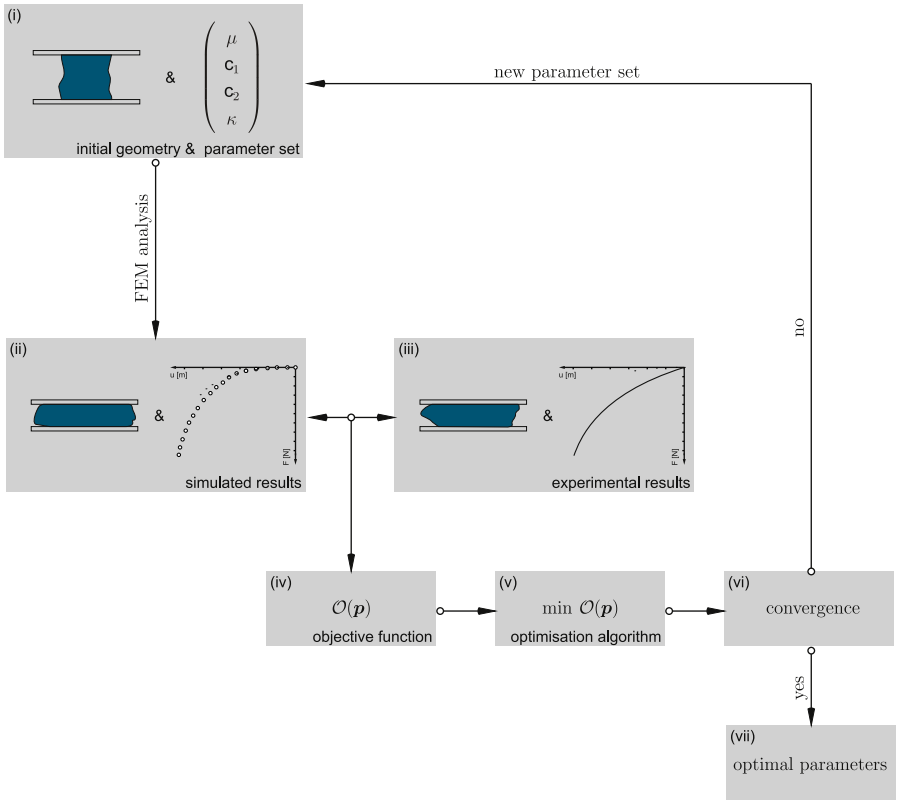

Fig. 4. Schematic illustration of the parameter identification algorithm.

Table 2
Fifteen optimised parameter sets based on the compression experiments. Note, the parameter c_2 has been fixed to be 70 during the identification process, as preliminary calculations indicated no appreciable variation of this parameter on the results. The mean values for the identified parameters are $\mu = 0.52 \pm 0.16$ kPa, $c_1 = 76.3 \pm 36.0$ kPa, and $\kappa = 0.15 \pm 0.05$, respectively.

Tissue set no.	μ (kPa)	c_1 (kPa)	c_2 (–)	κ (–)	$\mathcal{O}(\boldsymbol{p})$
I	0.6	111	70	0.1	0.02
II	0.5	30	70	0.1	0.04
III	0.3	43	70	0.2	0.02
IV	0.3	106	70	0.2	0.01
V	0.2	50	70	0.2	0.02
VI	0.4	78	70	0.2	0.03
VII	0.4	50	70	0.2	0.02
VII	0.8	101	70	0.2	0.03
IX	0.7	106	70	0.1	0.01
X	0.6	57	70	0.2	0.03
XI	0.6	30	70	0.1	0.03
XII	0.5	118	70	0.2	0.02
XIII	0.7	154	70	0.1	0.03
XIV	0.6	61	70	0.1	0.02
XV	0.6	50	70	0.1	0.03
Mean $\pm$ s.d.	**0.52 $\pm$ 0.16**	**76.3 $\pm$ 36.0**	**70.0 $\pm$ 0.0**	**0.15 $\pm$ 0.05**	**0.02 $\pm$ 0.01**

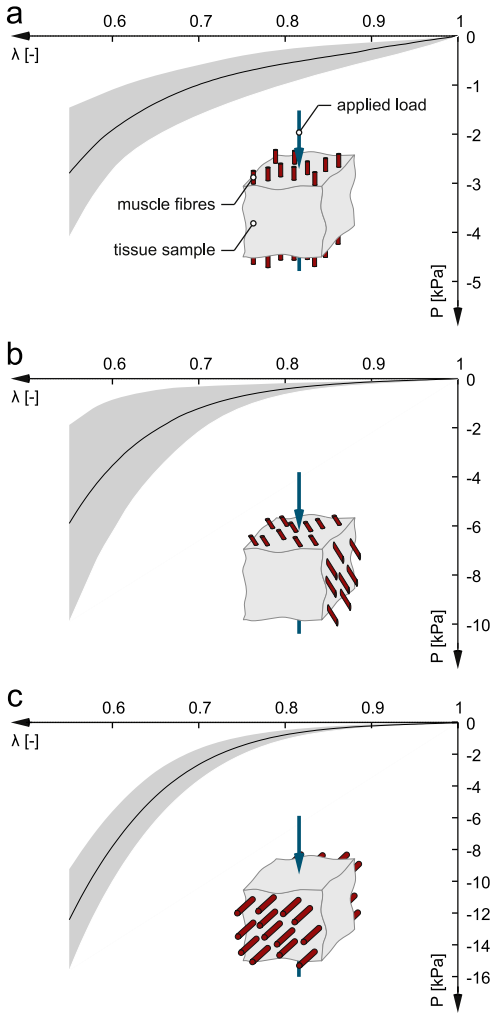

Fig. 5. Compressive stress–stretch responses of 37 muscle sample, c.f. Table 1, for loading directions of (a) 0°, (b) 45°, and (c) 90° with respect to the tissues' fibre direction, see subfigures. The black curves indicate mean values whereas the grey area depicts the standard deviation.

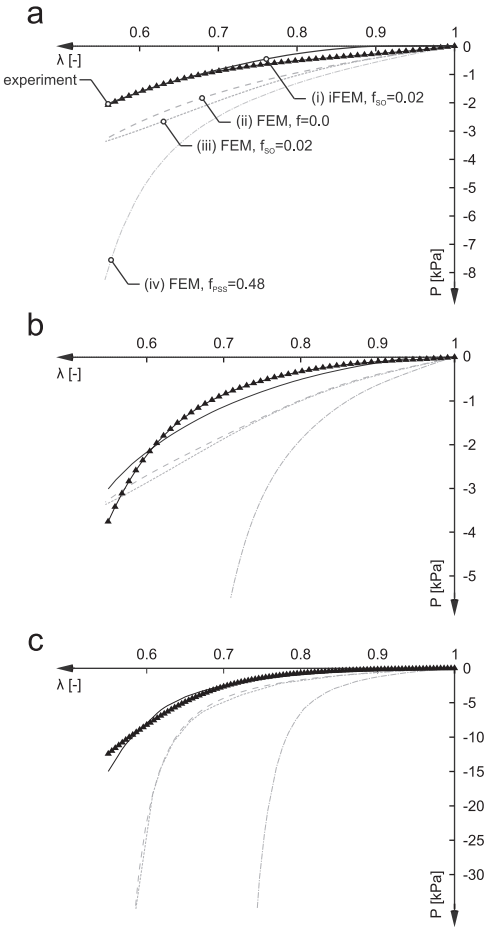

Fig. 6. Comparison between experiment, iFEM (i) and forward FEM (ii–iv) simulations for different static friction coefficients conducted on tissue sample I. Shown are the compressive stress–stretch behaviours for fibre orientations of (a) 0°, (b) 45°, and (c) 90° with respect to the loading direction according to the subfigures in Fig. 5. Note, for all simulations the optimised parameters of tissue set I, see Table 2, have been used.

In order to quantify both the deviation of the undeformed samples from an ideal cubic geometry and the difference between the simulated deformed shapes and the experimental ones, the measures Ω^j and Δ^j were introduced, respectively, where $j = 0°/45°/90°$. To this end, we calculated the distances ω of the nodes of the undeformed sample surface to a point on the face of the idealised cuboid lying in normal direction to the undeformed surface. Likewise the deflection δ, i.e. the distance between the nodal positions of the simulated and experimental deformed shapes, was calculated. The average values then obtained for each orientation j as

$$\Omega^j = \sum_{i=1}^{r} \frac{|\omega_i^j|}{r} \quad \text{and} \quad \Delta^j = \sum_{i=1}^{r} \frac{|\delta_i^j|}{r}, \tag{5}$$

where r represents the number of nodes without prescribed displacements. For the calculation of Ω^j this rules out nodes on the bottom face, for Δ^j nodes on the bottom and top face, which were in contact with the platens. The obtained values are provided in Table 3 together with their mean and standard deviation. Moreover, as an example, the deformed geometries of 0°, 45° and 90° specimens from sample I are displayed in Fig. 7(a)–(c), respectively, where the deflection δ is overlaid as contour plots. A positive value of δ indicates that the simulated nodal position lies further outward than the experimentally obtained one. The obtained deflections are generally less than 1 mm and the highest value occurs for the 90° direction (c). Based on the mean values, the smallest average deflection is obtained for 0° (0.24 ± 0.06 mm), whereas again the 90° direction shows the worst agreement with the experimentally obtained geometries (0.35 ± 0.01 mm).

In addition we calculated the average deflections Δ^j for the case in which a perfect cuboid shape was used as reference geometry (Fig. 6). The results are also given in Table 3 and highlight two issues: First, the average deflections are much higher, about twice as high as in the case where the real reference geometries are used. Second, similar to the aforementioned results, the best agreement is achieved for the 0° direction followed by the 45° and 90° direction.

4. Discussion

Testing of soft biological tissues is usually complicated by two major issues: It is nearly impossible to produce ideal sample geometries such as cuboids or cylinders and the exact boundary conditions applied to the samples are often unknown. For this reason, it is indispensable to gain detailed knowledge of how these two factors influence the measurements and finally the results of the parameter identification. In the present contribution the first point

Table 3
Mean and standard deviation of all samples in dependence on the fibre orientation. Mark '–': due to the dimension of the muscle no measurement was performed for this loading direction.

Tissue set no.	Ω^j (mm)			Δ^j (mm)		
	0°	45°	90°	0°	45°	90°
I	0.30	0.39	0.35	0.19	0.19	0.35
II	–	0.34	0.36	–	0.60	0.22
III	0.24	0.26	0.25	0.19	0.18	0.3
IV	–	0.37	0.27	–	0.15	0.57
V	–	0.46	0.44	–	0.23	0.28
VI	–	0.53	0.48	–	0.32	0.48
VII	0.30	0.4	0.37	0.19	0.34	0.32
VIII	0.53	0.59	0.38	0.24	0.26	0.35
IX	0.63	0.41	0.41	0.23	0.13	0.47
X	0.42	0.46	0.36	0.28	0.29	0.21
XI	0.50	0.37	–	0.37	0.30	–
XII	0.32	0.35	0.41	0.21	0.14	0.33
XIII	0.36	–	0.29	0.24	–	0.29
XIV	–	0.39	0.23	–	0.18	0.36
XV	–	0.41	0.29	–	0.23	0.23
Mean ± s.d.	**0.40 ± 0.12**	**0.41 ± 0.08**	**0.35 ± 0.07**	**0.24 ± 0.06**	**0.27 ± 0.13**	**0.35 ± 0.1**

Cuboid	Ω^j (mm)			Δ^j (mm)		
	0°	45°	90°	0°	45°	90°
$f = 0.00$	0.00	0.00	0.00	0.30	0.42	0.72
$f = 0.02$ (SO)	0.00	0.00	0.00	0.29	0.44	0.72
$f = 0.48$ (PSS)	0.00	0.00	0.00	0.29	0.39	0.61

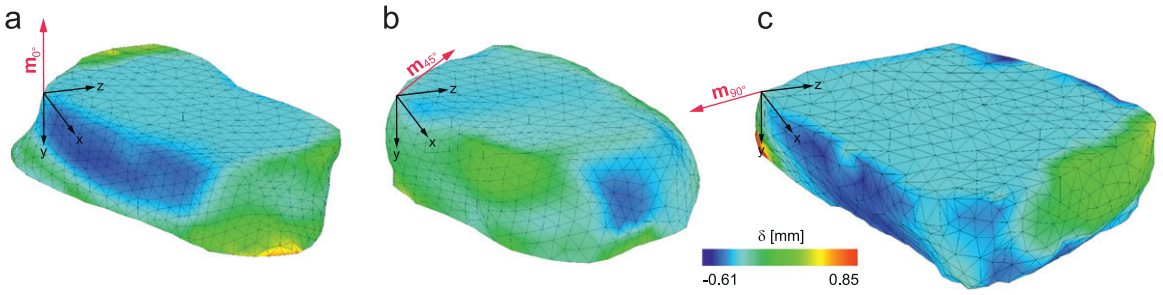

Fig. 7. Deflection δ in dependence on the fibre orientations: (a) 0°, (b) 45°, and (c) 90°, see arrows. For the simulations 3119 hybrid linear tetrahedral elements and 870 nodes on average have been used. In order to reflect the situation during testing, the axial displacements on the top and bottom faces were prescribed and hard contact including finite sliding was applied (Dassault Systèmes Simulia Corp., 2010).

was investigated by taking into account the real sample geometries before and at maximum compression using the iFEM for parameter identification instead of a simplified analytical solution. The agreement between simulation and experiment was not only very sound with regard to the force-displacement or, equivalently, compressive stress–stretch response but also with respect to the deformed shape of the samples. This is substantiated by the relatively small values of the objective function (4) representing the relative square error (Table 2) and the mean of the average deflections between 0.24 mm and 0.35 mm (Table 3). Bearing the complex sample geometries in mind, these values can be considered very satisfying. On the other hand, using the optimised parameter set in forward calculations with an idealised cuboid reference geometry and same static coefficient of friction f, the solution deviated substantially from the experimental results. The influence of friction between the sample surface and the platens was further studied by varying f in the FEM simulations. It has been seen that the value of f has a drastic influence on the numerical results and, particularly, that a high f results in a much stiffer response of the tissue. This can be explained by the fact that strong friction on the surface prevents the sample from extending laterally and thus causes severe bulging (Miller, 2001, 2005). For the 90° direction the influence on the compressive stress–stretch behaviour is particularly significant since bulging and incompressibility force fibres in the central area of the specimen to be more extended and the associated strain–energy (Eq. (3)) is strongly non-linear. Moreover, it is worth noting that the ideal cuboid sample with zero friction corresponds to an ideal uniaxial compression problem with lateral extension, which could also easily be solved analytically. Compared to the use of the original geometry and boundary conditions, this treatment represents a substantial simplification. Fig. 6 clearly underlines that, based on the same set of material parameters, the results between this 'analytic' and the more precise numerical solution are clearly different.

Concerning the experimental compressive response of passive muscle tissue, our results are partially in line with those obtained by Van Loocke et al. (2006) for orientation dependent compression of fresh and aged porcine muscle tissue. For the aged tissue the sequence of stiffness was the same as in Fig. 5, i.e. the stiffness increased with an increasing angle between compression and fibre direction. In contrast, for the fresh tissue they found that the samples with 45° fibre orientation yielded the softest response. Since we conducted the experiments with fresh tissue, i.e. within 2 h after animal death, we expect the disagreement to be due to variations between different muscles and species, and the fact that the fibre orientation may be less homogeneous in specimens prepared from the rabbit soleus muscle, which is small compared

to the porcine tissue used by Van Loocke et al. (2006). Nevertheless, all experiments agree in that the samples with fibres perpendicular to the loading direction yield the stiffest response. These results imply that the fibre contribution is much more distinct when they are subjected to tension than in a compressed state. To some extent, this justifies the constitutive assumption in Eq. (3) that the fibre contribution may be disregarded when the compressive stretch in the associated direction is less than one. The good agreement of the model in terms of compressive stress–stretch behaviour in Fig. 6(a) and the average deflection for 0° (0.24 ± 0.06 mm) provide further support for the applicability of this assumption for the tested tissue. Further, the comparison of the orientation angles' (α_m) standard deviation (6.9°,9.1°, and 2.7°) in Table 1 with the average relative standard deviations (0.63, 0.68, and 0.44) of the measured compressive stress–stretch behaviour in Section 3.1 shows a distinct correlation between both quantities and demonstrate the importance of accurate sample preparation.

Despite a generally good agreement, there are slight deviations between simulated and experimental compressive stress–stretch curves (Fig. 6). We attribute this to the choice of the constitutive model and remark that alternative representations (e.g. Böl et al., 2011; Ehret et al., 2011) may improve the fit. Moreover, we note that even with an advanced parameter identification technique, the use of compression tests alone is not sufficient to define the parameter set uniquely (c.f. Holzapfel and Ogden, 2009; Simms et al., 2012). As a critical point, we underline that the deflection between experimental and simulated tissue geometry was calculated post hoc. It seems evident that inclusion of the deflection into the objective function would lead to better results in terms of geometry agreement. This improvement is currently under work.

The main conclusion to be drawn from the present investigation is that knowledge of precise sample geometry and boundary conditions is extremely important when using the iFEM to identify material parameters. A parameter set identified from the simulation of a sample with real geometry generally yields a substantially different result when used with an idealised geometry. Moreover, the simulated results are very sensible to the coefficient of friction between sample and platens. The paper underlines that more attention should be spent to these two important aspects in experimental soft tissue mechanics.

Conflict of interest statement

All authors have no conflicts of interest.

Acknowledgements

Partial support for this research was provided by the Deutsche Forschungsgemeinschaft (DFG) under Grants BO 3091/4-1 and SI 841/3-1. The authors appreciate the support of J. Kirschbaum and R. Blickhan during this study. Further, we thank the anonymous reviewers for valuable comments on the previous versions of the manuscript.

References

Ahn, B., Kim, J., 2010. Measurement and characterization of soft tissue behavior with surface deformation and force response under large deformations. Medical Image Analysis 14 (2), 138–148.

Aimedieu, P., Mitton, D., Faure, J.P., Denninger, L., Lavaste, F., 2003. Dynamic stiffness and damping of porcine muscle specimens. Medical Engineering Physics 25 (9), 795–799.

Baskin, R.J., Paolini, P.J., 1967. Volume change and pressure development in muscle during contraction. American Journal of Physiology 213 (4), 1025–1030.

Böl, M., Weikert, R., Weichert, C., 2011. A coupled electromechanical model for the excitation-dependent contraction of skeletal muscle. Journal of the Mechanical Behavior of Biomedical Materials 4 (7), 1299–1310.

Calvo, B., Ramírez, A., Alonso, A., Grasa, J., Soteras, F., Osta, R., Muñoz, M.J., 2010. Passive nonlinear elastic behaviour of skeletal muscle: experimental results and model formulation. Journal of Biomechanics 43 (2), 318–325.

Chawla, A., Mukherjee, S., Karthikeyan, B., 2009. Characterization of human passive muscles for impact loads using genetic algorithm and inverse finite element methods. Biomechanics and Modeling in Mechanobiology 8 (1), 67–76.

Dassault Systèmes Simulia Corp., 2010. Abaqus 6.10 Unified Finite Element System 〈www.simulia.com〉.

Ehret, A.E., Böl, M., Itskov, M., 2011. A continuum constitutive model for the active behaviour of skeletal muscle. Journal of the Mechanics and Physics of Solids 59 (3), 625–636.

Gasser, T.C., Ogden, R.W., Holzapfel, G.A., 2006. Hyperelastic modelling of arterial layers with distributed collagen fibre orientations. Journal of the Royal Society Interface 3 (6), 15–35.

Hollenstein, M., Ehret, A.E., Itskov, M., Mazza, E., 2011. A novel experimental procedure based on pure shear testing of dermatome-cut samples applied to porcine skin. Biomechanics and Modeling in Mechanobiology 10 (5), 651–661.

Holzapfel, G.A., Ogden, R.W., 2009. On planar biaxial tests for anisotropic nonlinearly elastic solids. A continuum mechanical framework. Mathematics and Mechanics of Solids 14 (5), 474–489.

Holzapfel, G.A., Gasser, T.C., Ogden, R.W., 2000. A new constitutive framework for arterial wall mechanics and a comparative study of material models. Journal of Elasticity 61 (1–3), 1–48.

Lagarias, J.C., Reeds, J.A., Wright, M.H., Wright, P.E., 1998. Convergence properties of the Nelder–Mead simplex method in low dimensions. SIAM Journal on Optimization 9 (1), 112–147.

McElhaney, J.H., 1966. Dynamic response of bone and muscle tissue. Journal of Applied Physiology 21 (4), 1231–1236.

Miller, K., 2001. How to test very soft biological tissues in extension? Journal of Biomechanics 34 (5), 651–657.

Miller, M., 2005. Method of testing very soft biological tissues in compression. Journal of Biomechanics 38 (1), 153–158.

Morriss, L., Wittek, A., Miller, K., 2008. Compression testing of very soft biological tissues using semi-confined configuration—a word of caution. Journal of Biomechanics 41 (1), 235–238.

Nava, A., Mazza, E., Furrer, M., Villiger, P., Reinhart, W.H., 2008. In vivo mechanical characterization of human liver. Medical Image Analysis 12 (2), 203–216.

Nelder, J.A., Mead, R., 1965. A simplex method for function minimization. The Computer Journal 7 (4), 308–313.

Nie, X., Cheng, J.I., Chen, W.W., Weerasooriya, T., 2011. Dynamic tensile response of porcine muscle. Journal of Applied Mechanics 78 (2), 1–5.

Ogden, R.W., 1997. Non-linear Elastic Deformations. Dover Publications, Mineola, NY.

Samur, E., Sedef, M., Basdogan, C., Avtan, L., Duzgun, O., 2007. A robotic indenter for minimally invasive measurement and characterization of soft tissue response. Medical Image Analysis 11 (4), 361–373.

Shacham, S., Castel, D., Gefen, A., 2010. Measurements of the static friction coefficient between bone and muscle tissues. Journal of Biomechanical Engineering 132 (8) 084502-4.

Simms, K.C., Van Loocke, M., Lyons, C.G., 2012. Skeletal muscle in compression: modelling approaches for the passive muscle bulk. Journal of Multiscale Computational Engineering 10 (2), 143–154.

van Sligtenhorst, C., Cronin, D.S., Wayne Brodland, G., 2006. High strain rate compressive properties of bovine muscle tissue determined using a split Hopkinson bar apparatus. Journal of Biomechanics 39 (10), 1852–1858.

Song, B., Chen, W., Ge, Y., Weerasooriya, T., 2007. Dynamic and quasi-static compressive response of porcine muscle. Journal of Biomechanics 40 (13), 2999–3005.

van Turnhout, M., Peters, G., Stekelenburg, A., Oomens, C., 2005. Passive transverse mechanical properties as a function of temperature of rat skeletal muscle in vitro. Biorheology 42 (3), 193–207.

Van Loocke, M., Lyons, C.G., Simms, C.K., 2006. A validated model of passive muscle in compression. Journal of Biomechanics 39 (16), 2999–3009.

Van Loocke, M., Lyons, C.G., Simms, C.K., 2008. Viscoelastic properties of passive skeletal muscle in compression: stress–relaxation behaviour and constitutive modelling. Journal of Biomechanics 41 (7), 1555–1566.

Van Loocke, M., Simms, C.K., Lyons, C.G., 2009. Viscoelastic properties of passive skeletal muscle in compression—cyclic behaviour. Journal of Biomechanics 42 (8), 1038–1048.

Yoo, L., Kim, H., Gupta, V., Demer, J.L., 2009. Quasilinear viscoelastic behavior of bovine extraocular muscle tissue. Investigative Ophthalmology & Visual Science 50 (8), 3721–3728.